J Eng Math (2008) 61:35–54
DOI 10.1007/s10665-007-9201-3

Moisture transport in fibrous clothing assemblies

Huaxiong Huang · Changhua Ye · Weiwei Sun

Received: 27 July 2006 / Accepted: 27 September 2007 / Published online: 18 October 2007

Abstract In this paper, moisture transport in fibrous clothing assemblies is investigated in a one-dimensional setting. A multi-component, multi-phase flow model in a fibrous porous medium with phase change is proposed. The model is a generalization of a single-component model used in a previous study by taking the air resistance to moisture transport into account. Capillary effect on liquid water motion is also included in the model. Using dimensional analysis, it is shown that there exist several different time scales. As a result, the fast-scale moisture transport is coupled with the energy equation while accumulation of liquid water in the pore and absorption of water by the fibers occur at slower time scales. By exploring scale separation, computations can be greatly simplified by decoupling these physical processes. An efficient semi-implicit numerical scheme is proposed for solving the gas (vapor and air) and energy equations, while the water equations are solved separately. At the time scale of experimental measurement, a quasi-steady approximate solution is also derived for gas concentration and temperature as a benchmark for numerical computation. Qualitative comparison between the numerical solutions and experimental measurements are also given. The results show that the new multi-component model proposed in this study gives a better prediction of total water accumulation near the outer boundary of the clothing assemblies.

Keywords Clothing assemblies · Condensation/evaporation · Fibrous porous medium · Multi-component flow · Multi-phase

1 Introduction

Mass and heat transfer in fibrous porous media can be found in numerous industrial and engineering applications, such as textile [1], paper and pulp [2], building materials [3,4], and more recently in the electrodes of

H. Huang (✉)
Department of Mathematics & Statistics, York University, Toronto, ON, Canada M3J 1P3
e-mail: hhuang@yorku.ca

C. Ye · W. Sun
Department of Mathematics, City University of Hong Kong, Kowloon, Hong Kong
e-mail: cye@math.cityu.edu.hk

W. Sun
e-mail: maweiw@math.cityu.edu.hk

proton-exchange membrane fuel cells [5]. In these applications, modeling becomes increasingly important since it provides an efficient and cost-effective way for evaluating new designs or testing new materials.

Previous work on modeling of coupled heat and moisture transfer with phase change in fibrous insulation can be found in [6–16]. Due to recent interests in PEM fuel cells, multi-component modeling and mathematical analysis have also been carried out for reactant and moisture transport in hydrophobic fibrous media when it is relevant [17,18]. In the context of fibrous clothing assemblies, Fan et al. [19–21] introduced dynamic moisture absorption and radiation heat transfer into the existing models and consequently they achieved better agreement with experimental measurements.

Even though the physical models are similar in these applications, there exist unique characteristics for each problem. In this paper, we will focus our attention on fibrous clothing assemblies. In particular, our model will be based on the one used in [21] as detailed experimental measurements are available for temperature and liquid water (ice) distribution inside three-layer clothing assemblies [22].

The purpose of the current paper is twofold. Our main objective is to develop a realistic mathematical model for moisture transport in porous clothing assemblies. In [21], it was assumed that the relative motion between air and vapor is small and, as a consequence, a single-component model was used. However, it can be verified that under the experimental conditions given in [21], the air-vapor mixture velocity given by Darcy's law is unrealistically large. On the other hand, in the experimental setup [22], only vapor is present on the warm side of the clothing assemblies. Due to the difference in the saturated vapor pressure between the two sides of the clothing assemblies, vapor flows from the warm side to the cold side, while air plays only a passive role. It is, therefore, closer to physical reality to treat vapor and air as two components, as air may provide significant resistance to vapor movement. Our other objective is to identify dominant physical processes and their relative time scales so that proper numerical methods can be applied. Even though we are also interested in developing efficient numerical methods for a class of problems related to mass transport in fibrous porous media, in this paper we will concentrate on model development and analysis, while a more detailed discussion on numerics will be the subject of a future paper.

The rest of the paper is organized as follows. In Sect. 2, we will introduce the mathematical model and the setup of the problem. We will restrict to a three-layer assembly in a one-dimension setting. Proper non-dimensionalization will be carried out and boundary conditions will be discussed. In Sect. 3 we discuss solution methodologies. We propose a semi-implicit finite-volume method which avoids iteration, yet has a good stability property. This is achieved by treating the convective term in the vapor equation more carefully. An approximate solution is derived by assuming a quasi-steady state. In Sect. 4, numerical solutions will be presented as well as qualitative comparisons with experiments. We will conclude the paper by a short summary and a discussion on future research in Sect. 5.

2 Problem description

The experimental setup discussed in [21] and [22] consists of a three-layer porous cloth assembly, as illustrated in Fig. 1. The outside cover of the assembly is exposed to air with fixed temperature and relative humidity, while the inside cover is exposed to an artificial human body with only vapor at a higher temperature and a higher relative humidity. The original model in [2] used diffusion as the main mechanism for water (vapor and liquid) transport inside the clothing assembly. It was subsequently modified by including convection due to a difference in vapor pressure. In both cases air motion has been ignored. As a result, the vapor speed is a few orders of magnitude higher than that found in [10] where convective and diffusive transports were of the same order.

In this study, we include relative air motion in our model. Intuitively, there exist several possible scenarios. If background mixture pressures on both side of the assembly are maintained at atmospheric pressure, vapor transport will be mainly due to diffusion and the model in [2] is justified. On the other hand, if the mixture pressures on both side of the assemblies are different but the values stay unchanged, a convective mechanism must be added and the velocity of the mixture may be assumed to be a constant, as in [10]. It is also possible that the vapor on one side of the assembly is generated quickly while the air pressure does not have time to adjust. The mixture velocity in this case will be determined by the vapor pressure only, which is the assumption made in [21]. However, it may not

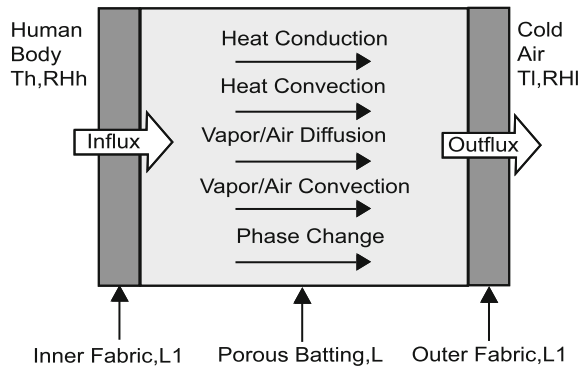

Fig. 1 Schematic diagram of the porous clothing ensemble used in an experimental study reported in [21,22]

be completely realistic to assume that the air will stay unchanged over a long period of time, especially when the vapor-pressure difference is significant.

While the above scenarios may be applicable under special conditions, it is more realistic to include air motion, as it provides extra resistance to vapor movement. Another reason for treating air and vapor separately is that they behave differently at the presence of the cover layer of the clothing assembly. For example, the resistance of the cover layer to air is often much larger than that to vapor [22]. The air in the inner layer of the assembly will be depleted due to outward convection, which in turn will reduce the convective speed of the mixture, since it depends on the pressure of the mixture, not that of vapor alone. As a consequence, the convective speed should be smaller than the one predicted by vapor pressure alone.

2.1 Mathematical model

We now write down the conservation of mass for vapor, air, and liquid, as well as conservation of energy for the mixture of gas, liquid and solid matrix as follows.

$$\frac{\partial}{\partial t}(\epsilon C_v) + \frac{\partial}{\partial x}(u_g \epsilon C_v) = \frac{\partial}{\partial x}\left(\frac{D_g \epsilon}{\tau_c} C \frac{\partial}{\partial x}\left(\frac{C_v}{C}\right)\right) - \Gamma, \tag{1}$$

$$\frac{\partial}{\partial t}(\epsilon C_a) + \frac{\partial}{\partial x}(u_g \epsilon C_a) = \frac{\partial}{\partial x}\left(\frac{D_g \epsilon}{\tau_c} C \frac{\partial}{\partial x}\left(\frac{C_a}{C}\right)\right), \tag{2}$$

$$\frac{\partial}{\partial t}(C_{vt} T) + \frac{\partial}{\partial x}\left(u_g \epsilon C_{vg} T\right) = \frac{\partial}{\partial x}\left(\kappa \frac{\partial T}{\partial x}\right) + \lambda M \Gamma, \tag{3}$$

$$\frac{\partial}{\partial t}\left(\rho(1-\epsilon')\widetilde{W}\right) + \frac{\partial(u_w \rho_w)}{\partial x} = \frac{\partial}{\partial x}\left(\rho(1-\epsilon') D_l \frac{\partial \widetilde{W}}{\partial x}\right) + M \Gamma_{ce}. \tag{4}$$

Here the generalized Fick's law [23, pp. 50–66] has been used for the binary multi-component gas mixture (vapor and air). C_v, C_a and $C = C_v + C_a$ are vapor, air and total (molar) concentrations, $\widetilde{W}$ is the liquid water content (%) on the fiber surface and u_g is the molar averaged mixture velocity. D_g and D_l are the molecular diffusion coefficient for gas (air and vapor) and liquid phases, respectively; τ_c is the tortuosity of the porous medium; C_{vt} and C_{vg} are the effective volumetric heat capacity and the heat capacity of the gas mixture (air and vapor), respectively; κ is the effective heat conductivity; λ is the latent heat of phase change (evaporation, condensation, and freezing); Γ is the (molar) rate of phase change per unit volume and M is the molecular weight of water. Since the effect of radiative heat transfer is small compared to that of heat conduction, it is not included in our model.

In addition, ρ_w and ρ are the water and fiber densities, respectively. The porosity with liquid water content (ϵ) and without liquid water content (ϵ') are related by

$$\epsilon = \epsilon' - \frac{\rho}{\rho_w}\widetilde{W}(1-\epsilon'). \tag{5}$$

The phase-change rate Γ consists of two parts $\Gamma = \Gamma_{ce} + \Gamma_s$, where

$$\Gamma_s = (1-\epsilon)\frac{\partial C_f}{\partial t} \tag{6}$$

is the rate due to absoption by the fiber and

$$\Gamma_{ce} = -\frac{E}{R_f}\sqrt{\frac{(1-\epsilon)(1-\epsilon')}{2\pi RM}}\left(\frac{P_{\text{sat}}}{\sqrt{T_s}} - \frac{P_v}{\sqrt{T_v}}\right) \tag{7}$$

is the Hertz–Knudsen equation [24, pp. 25–43] for condensation and evaporation (molar rate). The vapor pressure is given by

$$P_v = RC_vT, \tag{8}$$

where R is the universal gas constant. The saturation pressure P_{sat} is determined from experimental measurements and fitted as

$$P_{\text{sat}} = \begin{cases} 651\text{e}^{0.072\Delta T} - 35, & T \le 275.5\ \text{K}, \\ 966\text{e}^{0.052\Delta T} - 398, & T > 275.5\ \text{K}, \end{cases} \tag{9}$$

with $\Delta T = T - T_0$ and $T_0 = 273$ K. Here we assume that $T_s = T_v = T$.

The amount of water absorbed by fiber with radius R_f, in mole per unit volume, is given by

$$C_f = \frac{2}{R_f^2}\int_0^{R_f} C_f' r\,\mathrm{d}r \tag{10}$$

and

$$\frac{\partial C_f'}{\partial t} = \frac{1}{r}\frac{\partial}{\partial r}\left(D_f r\frac{\partial C_f'}{\partial r}\right) \tag{11}$$

with $C_f'(R_f, t) = \rho W_f'(RH)/M$ and $W_f'(RH)$ (water content relative the fiber density ρ) is available via experimental measurements. In this paper we will also use relative humidity defined by $RH = P_v/P_{\text{sat}}$.

The effective heat conductivity κ is given by

$$\kappa = \epsilon\kappa_v + (1-\epsilon)\left(\kappa_f + \frac{\rho}{\rho_w}W\kappa_w\right)\left(1 + \frac{\rho}{\rho_w}W\right)^{-1} \tag{12}$$

and

$$C_{vt} = \epsilon C_{vg} + (1-\epsilon)\left(C_{vf} + \frac{\rho}{\rho_w}WC_{vw}\right)\left(1 + \frac{\rho}{\rho_w}W\right)^{-1} \tag{13}$$

is the effective volumetric heat capacity. Here κ_v, κ_w, and κ_f are the heat conductivity for gas (air and vapor), water and fiber, C_{vg}, C_{vf}, and C_{vw} are heat capacity for gas, fiber, and water, respectively. W is the total volumetric water content (%) absorbed by the fiber and on the fiber surface, i.e.,

$$W = \widetilde{W} + W_f, \quad W_f = \frac{MC_f}{\rho} = \frac{2M}{\rho R^2}\int_0^R C_f' r\,\mathrm{d}r. \tag{14}$$

Finally the vapor–air mixture velocity (volumetric discharge) is given by Darcy's law

$$u_g = -\frac{kk_{rg}}{\mu_g}\frac{\partial P_g}{\partial x}, \tag{15}$$

where k is the permeability, k_{rg} and μ_g are the relative permeability and the viscosity of the gas mixture, respectively. $P_g = P_v + P_a$ is the total gas pressure. The water volumetric discharge (velocity) is given similarly as

$$u_w = -\frac{kk_{rw}}{\mu_w}\frac{\partial P_w}{\partial x}, \tag{16}$$

where k_{rw} is the relative permeability and μ_w is the viscosity of the water. The liquid water pressure is given by $P_w = P_g - P_c \approx -P_c$ by neglecting the total gas pressure and the capillary pressure is given in [25] as

$$P_c = \sigma \sqrt{\frac{k}{\epsilon'}} J(s), \tag{17}$$

where

$$J(s) = 1.417(1-s) - 2.120(1-s)^2 + 1.263(1-s)^3;$$

here σ is the surface tension and s is the volumetric liquid saturation in the inter fiber void space, which is related to the water content by

$$s = \frac{(1-\epsilon')\rho \widetilde{W}}{\epsilon' \rho_w}. \tag{18}$$

For the relative permeability we use empirical relations $k_{rw} = s^3$ and $k_{rg} = (1-s)^3$.

2.2 Boundary conditions

Boundary conditions are usually dictated by the settings of the problems. Here we will follow the experimental setup described in [22] closely. As the clothing assembly is placed on an artificial skin which is a porous water-proof layer in direct contact with water and the water container is sealed off from the air supplies, we assume that the vapor is fully saturated, while there is no air flux at the inner boundary ($x = 0$). More precisely, we have

$$q_v^i = h_v^i (C_v^i - C_v), \quad q_a^i = h_a^i (C_a^i - C_a), \tag{19}$$

where h_v^i and h_a^i are the mass-transfer coefficients for for vapor and air, respectively. For air, we assume that $h_a^i = 0$ and for vapor we assume a relative humidity 100% due to constant evaporation, i.e., $RH = 1$. Therefore the vapor concentration can be computed using the following relationship

$$C_v^i = \frac{P_{\text{sat}}(T_H)}{RT_H}, \tag{20}$$

where $T_H = 303$ K is the "body" temperature. The boundary condition for temperature is simply $T = T_H$.

Outside the outer-cover layer of the assembly, we assume that the background temperature is fixed at a lower temperature $T_L = 253$ K with a relative humidity of RH_L (e.g., 90%) unless it is stated otherwise. The background vapor concentration can be calculated using the following equation

$$C_v^o = \frac{P_{\text{sat}}(T_L)}{RT_L}. \tag{21}$$

We also assume, following [21], that there exist resistances to both mass and heat fluxes, i.e., we have

$$q_v^o = h_v^o (C_v - C_v^o), \quad q_a^o = h_a^o (C_a - C_a^o), \quad q_t^o = h_t^o (T - T_L), \tag{22}$$

where h_v^o and h_a^o are mass-transfer coefficients for the vapor and air, respectively, and h_t^o is the heat-transfer coefficient. We assume that the background air pressure is the atmospheric pressure P_{atm}, from which the air concentration can be calculated as

$$C_a^o = \frac{P_{\text{atm}}}{RT_L}. \tag{23}$$

For the water content the boundary condition may vary, depending on the circumstances. For example, we can use $\widetilde{W} = 0$ or zero fluxes $q_w = 0$ at both ends.

2.3 Non-dimensionalization

We non-dimensionalize the equations by using the following scalings:

$$c = \frac{C}{C_v^i} = c_1 + \phi c_2, \quad \phi = \frac{C_a^o}{C_v^i}, \quad c_1 = \frac{C_v}{C_v^i}, \quad c_2 = \frac{C_a}{C_a^o}, \quad c_f = \frac{C_f}{C_v^i}, \quad \theta = \frac{T}{T_0}, \quad p_s = \frac{P_{\text{sat}}}{P_{\text{sat}}(T_H)},$$
$$p_v = \frac{P_v}{RC_v^i T_0}, \quad \xi = \frac{x}{L}, \ \tau = \frac{t}{\bar{t}}.$$

Here $\bar{t}$ is the reference time to be determined. The governing equations in non-dimensional form are

$$\frac{\partial(\epsilon c_1)}{\partial \tau} + \frac{\partial(\bar{v}_G \epsilon c_1)}{\partial \xi} = \frac{\partial}{\partial \xi}\left(\delta_G \epsilon c \frac{\partial}{\partial \xi}\left(\frac{c_1}{c}\right)\right) - \beta_G S - (1-\epsilon')\frac{\partial c_f}{\partial \tau}, \tag{24}$$

$$\frac{\partial(\epsilon c_2)}{\partial \tau} + \frac{\partial(\bar{v}_G \epsilon c_2)}{\partial \xi} = \frac{\partial}{\partial \xi}\left(\delta_G \epsilon c \frac{\partial}{\partial \xi}\left(\frac{c_2}{c}\right)\right), \tag{25}$$

$$\frac{\partial(c_{vt}\theta)}{\partial \tau} + \frac{\partial(\bar{v}_T \epsilon \theta)}{\partial \xi} = \frac{\partial}{\partial \xi}\left(\delta_T \kappa_T \frac{\partial \theta}{\partial \xi}\right) + \beta_T S + \phi_T (1-\epsilon')\frac{\partial c_f}{\partial \tau}, \tag{26}$$

$$\frac{\partial\left(\rho_{fw}(1-\epsilon')\widetilde{W}\right)}{\partial \tau} + \frac{\partial \bar{v}_W}{\partial \xi} = \frac{\partial}{\partial \xi}\left(\delta_W \rho_{fw}(1-\epsilon')\frac{\partial \widetilde{W}}{\partial \xi}\right) + \beta_W S, \tag{27}$$

where

$$\bar{v}_G = -v_G \frac{\partial(c\theta)}{\partial \xi}, \tag{28}$$

$$\bar{v}_T = -v_T \frac{\partial(c\theta)}{\partial \xi}, \tag{29}$$

$$\bar{v}_W = v_W \widetilde{W}^3 J_s(s) \frac{\partial \widetilde{W}}{\partial \xi}, \tag{30}$$

$$p_s(\theta) = \begin{cases} 0.675 p_{s0}(\mathrm{e}^{1.37\alpha(\theta-1)} - 0.0538), & \theta < \theta_c \\ p_{s0}\left(\mathrm{e}^{\alpha(\theta-1)} - 0.412\right), & \theta \geq \theta_c \end{cases} \tag{31}$$

$$J_s(s) = -1.42 + 4.24(1-s) - 3.79(1-s)^2, \tag{32}$$

$$S = (1-\epsilon')\sqrt{1+\rho_{fw}\widetilde{W}}\frac{c_1\theta - p_s(\theta)}{\sqrt{\theta}}, \tag{33}$$

$$c_v = \frac{C_v}{C_{vf}} = \epsilon c_{vaf} + (1-\epsilon)\frac{1+\rho_{fw}W c_{vwf}}{1+\rho_{fw}W}, \tag{34}$$

$$\kappa_T = \frac{\kappa}{\kappa_f} = \epsilon \kappa_{vf} + (1-\epsilon)\frac{1+\rho_{fw}W\kappa_{wf}}{1+\rho_{fw}W}. \tag{35}$$

Note that $J_s(s)$ is strictly negative for $0 \leq s \leq 1$.

The boundary conditions at $\xi = 0$ are

$$-v_G \epsilon c_1 \frac{\partial(c\theta)}{\partial \xi} - \delta_G \epsilon c \frac{\partial}{\partial \xi}\left(\frac{c_1}{c}\right) = \frac{1}{R_{c_{1H}} + 1/h_{c_{1H}}}(c_{1H} - c_1), \tag{36}$$

$$-v_G \epsilon c_2 \frac{\partial(c\theta)}{\partial \xi} - \delta_G \epsilon c \frac{\partial}{\partial \xi}\left(\frac{c_2}{c}\right) = \frac{1}{R_{c_{2H}} + 1/h_{c_{2H}}}(c_{2H} - c_2), \tag{37}$$

$$-v_T \epsilon \theta \frac{\partial(c\theta)}{\partial \xi} - \delta_T \kappa_T \frac{\partial \theta}{\partial \xi} = \frac{1}{R_{T_H} + 1/h_{T_H}}(\theta_H - \theta), \tag{38}$$

$$v_W \widetilde{W}^3 J_s(s) \frac{\partial \widetilde{W}}{\partial \xi} - \delta_W \rho_{fw}(1-\epsilon')\frac{\partial \widetilde{W}}{\partial \xi} = 0, \tag{39}$$

where $R_{c_{1H}}$ and $R_{c_{2H}}$ are the non-dimensional mass resistances for vapor and air, respectively; R_{T_H} is the non-dimensional thermal resistance, $h_{c_{1H}}$ and $h_{c_{2H}}$ are the nondimensional mass transfer coefficients, and h_{T_H} is the non-dimensional heat-transfer coefficient. At $\xi = 1$, the conditions are similar

$$-v_G \epsilon c_1 \frac{\partial(c\theta)}{\partial \xi} - \delta_G \epsilon c \frac{\partial}{\partial \xi}\left(\frac{c_1}{c}\right) = \frac{1}{R_{c_{1L}} + 1/h_{c_{1L}}}(c_1 - c_{1L}), \tag{40}$$

$$-v_G \epsilon c_2 \frac{\partial(c\theta)}{\partial \xi} - \delta_G \epsilon c \frac{\partial}{\partial \xi}\left(\frac{c_2}{c}\right) = \frac{1}{R_{c_{2L}} + 1/h_{c_{2L}}}(c_2 - c_{2L}), \tag{41}$$

$$-v_T \epsilon \theta \frac{\partial(c\theta)}{\partial \xi} - \delta_T \kappa_T \frac{\partial \theta}{\partial \xi} = \frac{1}{R_{T_L} + 1/h_{T_L}}(\theta - \theta_L), \tag{42}$$

$$v_W \widetilde{W}^3 J_s(s) \frac{\partial \widetilde{W}}{\partial \xi} - \delta_W \rho_{fw}(1 - \epsilon') \frac{\partial \widetilde{W}}{\partial \xi} = 0, \tag{43}$$

where $h_{c_{1L}}$ and $h_{c_{2L}}$ are the non-dimensional mass-transfer coefficients and h_{T_L} is the non-dimensional heat-transfer coefficient. The resistance coefficients of the cover layer for vapor, air and heat are $R_{c_{1L}}$, $R_{c_{2L}}$ and R_{T_L}, respectively. Note that we have assumed that there is no flux of liquid water (or ice) through the boundaries.

We have listed the values of the physical and geometric parameters in Table 1, the definition of the non-dimensional parameters and their values are given in Table 2.

Table 1 Values of physical parameters

Parameter	Batting (polyester)	Lining/cover	Unit
ρ in (5)	1.39×10^3	Unchanged	kg/m^3
ρ_w in (5)	1×10^3	–	–
ϵ' in (5)	0.993	0.1	
λ in (3)	2.26×10^6	Unchanged	J/kg
τ_c in (1)	1.2	1.05	
D_g in (1)	2.5×10^{-5}	Unchanged	m^2/s
D_l in (4)	1.35×10^{-13}	–	–
D_f in (11)	1.0×10^{-16}	–	–
E in (7)	2.4×10^{-6}	–	
κ_v in (12)	2.5×10^{-2}	–	Wm^{-1}K^{-1}
κ_w (water) in (12)	5.7×10^{-1}	–	–
κ_w (ice) in (12)	2.13-0.0132ΔT	–	–
κ_f in (12)	1×10^{-1}	0.1	–
C_{vg} in (13)	1.169×10^3	Unchanged	Jm^{-1}K^{-1}
C_{vf} in (13)	1.3×10^6	–	–
C_{vw} in (13)	4.2×10^6	–	–
k in (15)	2.2×10^{-10}	1.1×10^{-13}	m^2
μ_g in (15)	2.2×10^{-5}	Unchanged	kg/m s
μ_w in (16)	2.5×10^{-4}	–	–
σ	7.24×10^{-2}	–	kg/s
L	4.92×10^{-3}	1×10^{-4}	m
R_f in (fiber radius)	1.03×10^{-5}	Unchanged	–
$T(x, 0)$	293	–	K
$RH(x, 0)$	65%	–	
$\widetilde{W}(x, 0)$	0	–	

Table 2 Non-dimensional parameters and their values, based on $\bar{t} = 1$ second

Parameter	Definition	Batting(polyester)	Lining/cover
ρ_{fw}	$\frac{\rho}{\rho_w}$	1.39	–
c_{vwf}	$\frac{C_{vw}}{C_{vf}}$	3.23	–
c_{vaf}	$\frac{C_{va}}{C_{vf}}$	8.88×10^{-4}	–
κ_{vf}	$\frac{\kappa_v}{\kappa_f}$	2.5×10^{-1}	–
κ_{wf}	$\frac{\kappa_w}{\kappa_f}$	5.7	–
β	$\frac{EC_v^i \bar{t}}{R_f}\sqrt{\frac{RT_0}{2\pi M}}$	5.56×10^{1}	–
v_G	$\frac{k(1-s)^3 RC_v^i T_0 \bar{t}}{\mu_a L^2}$	15.8	2.3×10^{1}
δ_G	$\frac{D_a \bar{t}}{\tau_c L^2}$	8.6×10^{-3}	2.38×10^{3}
α	$0.052227 T_0$	1.4258×10^{1}	–
β_G	$\frac{\beta}{C_v^i}$	3.3×10^{1}	–
v_T	$v_G c_{vaf}$	1.4×10^{-2}	2.066
δ_T	$\frac{\kappa_f \bar{t}}{C_{vf} L^2}$	3.18×10^{-5}	7.69×10^{3}
β_T	$\frac{\lambda \beta M}{T_0 C_{vf}}$	$6.4 \times 10^{-3} (T \geq 273)$	–
		$7.3 \times 10^{-3} (T < 273)$	–
ϕ_T	$\frac{\lambda C_v^i}{T_0 C_{vf}}$	$1.1 \times 10^{-2} (T \geq 273)$	–
		$1.3 \times 10^{-2} (T < 273)$	–
v_W	$\frac{\sigma k \bar{t}}{\mu_w L^2}\sqrt{\frac{k}{\epsilon'}}\left(\rho_{fw}\frac{1-\epsilon'}{\epsilon'}\right)^4$	3.61×10^{-18}	1.121×10^{8}
δ_W	$\frac{D_l \bar{t}}{L^2}$	5.58×10^{-11}	5.58×10^{-11}
β_W	$\frac{\beta M}{\rho_w}$	10^{-3}	–
p_{s0}	$1/[\exp(\alpha(\theta_H - 1)) - 398/966]$	0.228	–
θ_c	$\frac{275.5}{T_0}$	1.009	–

2.4 Time scales for the physical processes

The non-dimensional parameters introduced in the previous section and their values listed in Table 2 are the main basis for the following discussion. However, it is helpful to note that the actual physical process also depends on the boundary conditions.

As indicated by the ratios of $v_G/\beta_G \approx 0.5$ and $v_T/\beta_T \approx 10$, if the non-dimensional pressure drop $(c\theta)_\xi$ is order one, then the convection and the phase change would be the most dominant processes, which occur at the time scale of seconds to a tenth of a second. Since the cover/lining is highly resistant to both air and vapor movements, the pressure difference between the lining and cover layers will drop and eventually the convective and diffusive motions of the air will be in balance, and the vapor and air motions occur at the time scale determined by the diffusive constant $\delta_G^{-1} \approx 10^2$ s, despite the large Sherwood number $\mathrm{Sh} = v_G/\delta_G \approx 10^3$. The time scale for the phase change (condensation or evaporation), is about three orders of magnitudes faster than the diffusive scale, given by the ratio $\delta_G/\beta_G \approx 10^3$. Since the diffusive time scale is 10^2 s, phase change occurs at the scale of 0.1 s.

The conductive time scale for the temperature is given by $\delta_T^{-1} \approx 10^4$, which is longer. The Peclet number given by $\mathrm{Pe} = v_T/\delta_T \approx 10^4$ is also one order of magnitude bigger than the Sherwood number, indicating that the convective heat transfer also is an order of magnitude slower than that for the vapor and air motions. On the other hand, the diffusive time scale for liquid water (and ice) is given by $\delta_W^{-1} \approx 10^{11}$ s, which is much longer. The Sherwood number for the convective water movement $v_W/\delta_W \approx 10^{-7}$ is also much smaller than that for the vapor and air. Therefore, water accumulation is determined by local condensation and water transport due to convection (capillary motion) and diffusion is negligible.

In summary, the convective time scale for vapor and air is comparable to the diffusive time scale, except during the initial stage. Phase change is the most dominant process which occurs at a much faster time scale. Heat conduction is slower than the molecular diffusion of vapor and air. Water movement is negligible as it is much slower than the other relevant physical processes. The wide range of scale separation associated with these physical processes will be explored in several aspects in this study. First of all, vapor and air transport occur at a shorter time scale, compared to that (hours) of the experimental observations. Therefore, a quasi-steady state can be used for vapor and air transport equations. This motivated us to derive quasi-steady approximate solutions, which can be used as benchmarks for the numerical computations using the full equations. Second, it also allows us to apply an efficient numerical method by decoupling liquid water accumulation from the rest of the computation. Finally, for non-hygroscophic batting, such as polyester, for which the liquid water absorption by fiber is neglected, one can see a quasi-steady form by choosing certain reference time $\bar{t}$ since $\beta_G, \beta_T, \bar{v}_G, \bar{v}_T, \delta_G, \delta_T \sim \bar{t}$.

Before we move on to the discussion of solution methodologies, we note that a scaling analysis can also be applied to the process of water absorption by fibers in clothing assemblies. The key parameter which determines the time scale of water absorption is $\delta_f = D_f/R_f^2 = 10^{-6}$ where D_f and R_f are the diffusion coefficient for water in the fiber and fiber radius, respectively. Since $\delta_f \ll \delta_G$, the effect of fiber absorption is much smaller than that of the diffusion on the dynamics of vapor concentration in the inter-fiber void space, except initially when the rate of absorption is relatively large. Therefore, we can decouple the fiber-absorption calculation by dropping it from the transport equation. The total water content absorbed by fiber can be computed using the steady state solution of vapor concentration. We will come back to this point in Sect. 4.

3 Solution methodologies

3.1 Approximate solutions

Since vapor and temperature reach the steady state within a short period of time, this suggests that we can seek the solution of the quasi-steady version of the governing equations

$$(\bar{v}_G \epsilon c_1)_\xi = \left(\delta_G \epsilon c \left(\frac{c_1}{c}\right)_\xi\right)_\xi - \beta_G S, \tag{44}$$

$$(\bar{v}_G \epsilon c_2)_\xi = \left(\delta_G \epsilon c \left(\frac{c_2}{c}\right)_\xi\right)_\xi, \tag{45}$$

$$(\bar{v}_T \epsilon \theta)_\xi = \left(\delta_T \kappa_T \theta_\xi\right)_\xi + \beta_T S. \tag{46}$$

In order to gain useful insights we will choose the following set of simplified boundary conditions

$$\xi = 0: \ c_1 = c_{1H}, \quad \bar{v}_G \epsilon c_2 - \delta_G \epsilon c \left(\frac{c_2}{c}\right)_\xi = 0, \quad \theta = \theta_H;$$

$$\xi = 1: \ c_1 = c_{1L}, \quad c_2 = c_{2L}, \quad \theta = \theta_L$$

where air supply in the inner layer is assumed to be zero.

Integrating (45) and noting the flux boundary condition, we have

$$\bar{v}_G \epsilon c_2 = \delta_G \epsilon c \left(\frac{c_2}{c}\right)_\xi$$

and moreover, by noting the fact that $c = c_1 + \phi c_2$ and $c_1 \ll c$,

$$\bar{v}_G = \frac{\delta_G c}{c_2}\left(\frac{c_2}{c}\right)_\xi \approx -\delta_G\left(\frac{c_1}{c}\right)_\xi. \tag{47}$$

Since $\bar{v}_G = -v_G(c\theta)_\xi$,

$$v_G(c\theta - c_L\theta_L) \approx \delta_G\left(\frac{c_1}{c} - \frac{c_{1L}}{c_L}\right). \tag{48}$$

Solving the above equation gives

$$c\theta \approx c_L\theta_L - \frac{\delta_G c_{1L}}{v_G c_L} + \frac{\delta_G c_1\theta}{v_G c_L\theta_L}. \tag{49}$$

Substituting (47) in (44) and (46), we have

$$\frac{\delta_G\epsilon}{\beta_G}\left((c+c_1)\left(\frac{c_1}{c}\right)_\xi\right)_\xi = S, \tag{50}$$

$$\frac{v_T\delta_G\epsilon}{v_G\beta_T}\left(\theta\left(\frac{c_1}{c}\right)_\xi\right)_\xi + \frac{\delta_T\kappa_T}{\beta_T}\theta_{\xi\xi} = -S \tag{51}$$

3.1.1 Wet case

First we consider the case with water around the whole batting area. In this case

$$\frac{\delta_G\epsilon}{\beta_G} \ll 1, \quad \frac{v_T\delta_G\epsilon}{v_G\beta_T} \ll 1, \quad \text{and} \quad \frac{\delta_T\kappa_T}{\beta_T} \ll 1,$$

Eqs. (50) and (51) lead to $S \approx 0$, i.e.,

$$c_1\theta = p_s(\theta). \tag{52}$$

Eliminating S from (50) and (51) gives

$$\frac{\delta_G\epsilon}{\beta_G}\left((c+c_1)\left(\frac{c_1}{c}\right)_\xi\right)_\xi + \frac{v_T\delta_G\epsilon}{\beta_T v_G}\left(\theta\left(\frac{c_1}{c}\right)_\xi\right)_\xi + \frac{\delta_T\kappa_T}{\beta_T}\theta_{\xi\xi} = 0. \tag{53}$$

By noting fact that $c \gg c_1$ and the second term can be ignored, Eq. (53) becomes

$$\nu\left(c\left(\frac{c_1}{c}\right)_\xi\right)_\xi + \theta_{\xi\xi} = 0 \tag{54}$$

where $\nu = \delta_G\epsilon\beta_T/(\delta_T\kappa_T\beta_G) \ll 1$. The leading-order solution with respect to ν is

$$\tilde{\theta} = (\theta_L - \theta_H)\xi + \theta_H.$$

A more precise approximation (first-order with respect to ν) satisfies the following equation, by combining the second equation of (48) and (54),

$$\frac{v_G\epsilon\beta_T}{\delta_T\kappa_T\beta_G}(c(c\theta)_\xi)_\xi + \theta_{\xi\xi} = 0$$

or equivalently

$$\frac{v_G\epsilon}{\beta_G}c(c\theta)_\xi + \frac{\delta_T\kappa_T}{\beta_T}\theta_\xi = d_T\,.$$

However, the solution of the above equation cannot be expressed in a simple closed form. So we consider the following approximation

$$\frac{v_G\epsilon}{\beta_G}c\theta(c\theta)_\xi + \frac{\delta_T\kappa_T}{\beta_T}\theta\theta_\xi = d_T\tilde{\theta}\,,$$

which is obtained by multiplying the original equation by θ and replacing θ on the right-hand side by its leading-order approximation. This is justified since we are only interested in the leading approximation. Integrating the above equation, we have

$$\frac{v_G\epsilon}{\beta_G}\left((c\theta)^2-(c_H\theta_H)^2\right)+\frac{\delta_T\kappa_T}{\beta_T}\left(\theta^2-\theta_H^2\right)=2d_T\left(\frac{\theta_L-\theta_H}{2}\xi^2+\theta_H\xi\right), \tag{55}$$

where

$$d_T=\frac{\frac{v_G\epsilon}{\beta_G}((c_L\theta_L)^2-(c_H\theta_H)^2)+\frac{\delta_T\kappa_T}{\beta_T}(\theta_L^2-\theta_H^2)}{\theta_L+\theta_H}.$$

By (49),

$$(c\theta)^2-(c_H\theta_H)^2=\frac{2\delta_G}{v_G}\left(p_s(\theta)-p_s(\theta_H)\right)+\left(\frac{\delta_G}{v_Gc_L\theta_L}\right)^2\left(p_s^2(\theta)-p_s^2(\theta_H)\right).$$

Ignoring the last term in the above equation, we have

$$\begin{aligned}2d_T\left(\frac{\theta_L-\theta_H}{2}\xi^2+\theta_H\xi\right)=&\frac{2\delta_G\epsilon}{\beta_G}\frac{p_s(\theta_L)-p_s(\theta_H)}{\theta_L^2-\theta_H^2}\left(((\theta_L-\theta_H)\xi+\theta_H)^2-\theta_H^2\right)\\&+\frac{\delta_T\kappa_T}{\beta_T}\left(((\theta_L-\theta_H)\xi+\theta_H)^2-\theta_H^2\right).\end{aligned} \tag{56}$$

Equation (55) becomes

$$\begin{aligned}&\frac{2\delta_G\epsilon}{\beta_G}\left(p_s(\theta)-p_s(\theta_H)\right)+\frac{\delta_T\kappa_T}{\beta_T}\theta^2\\&=\frac{2\delta_G\epsilon}{\beta_G}\frac{(p_s(\theta_L)-p_s(\theta_H))}{\theta_L^2-\theta_H^2}\left(((\theta_L-\theta_H)\xi+\theta_H)^2-\theta_H^2\right)+\frac{\delta_T\kappa_T}{\beta_T}((\theta_L-\theta_H)\xi+\theta_H)^2.\end{aligned} \tag{57}$$

The temperature θ is defined implicitly by the above equation and c_1 and c are given in (52) and (49), respectively.

3.1.2 Dry case

When the batting is dry, no phase change occurs. Since the conduction in (51) is dominant ($\epsilon v_T\delta_G/v_G\beta_T\ll 1$), we have

$$\delta_T\kappa_T\theta_{\xi\xi}=0 \tag{58}$$

with the corresponding boundary conditions, which leads to the linear solution

$$\theta=\theta_L\xi+\theta_H(1-\xi).$$

Approximately, we can rewrite (50) into

$$\delta_G\epsilon\left(c\left(\frac{c_1}{c}\right)_\xi\right)_\xi=0\quad\text{or}\quad(c(c\theta)_\xi)_\xi=0$$

which gives

$$\theta^2c^2=\theta_H^2c_H^2+\frac{\theta_L^2c_L^2-\theta_H^2c_H^2}{\theta_L+\theta_H}\left(\theta_L\xi^2+\theta_H(1-(1-\xi)^2)\right)$$

and c_1 is given in (48).

3.1.3 Wet–dry case

For intermediate environment temperature, two phase zones appear in the batting. Based on the boundary conditions, it is reasonable to assume that the wet zone is located in $(0, \bar{\xi})$ and the dry zone is in $(\bar{\xi}, 1)$. Let $\bar{\theta} = \theta(\bar{\xi})$ and $\bar{c} = c(\bar{\theta})$. Then the solutions at wet zone and dry zone can be obtained from the above formulas and we rewrite them by

$$\frac{2\delta_G\epsilon}{\beta_G}(p_s(\theta) - p_s(\theta_H)) + \frac{\delta_T\kappa_T}{\beta_T}\theta^2 = \frac{2\delta_G\epsilon}{\beta_G}\frac{p_s(\bar{\theta}) - p_s(\theta_H)}{\bar{\theta}^2 - \theta_H^2}\left(\left((\bar{\theta} - \theta_H)\frac{\xi}{\bar{\xi}} + \theta_H\right)^2 - \theta_H^2\right) + \frac{\delta_T\kappa_T}{\beta_T}((\bar{\theta} - \theta_H)\frac{\xi}{\bar{\xi}} + \theta_H)^2, \tag{59}$$

$$c = \frac{1}{\theta}\left(c_L\theta_L - \frac{\delta_G c_{1L}}{v_G c_L} + \frac{\delta_G p_s(\theta)}{v_G c_L \theta_L}\right), \tag{60}$$

$$c_1 = \frac{p_s(\theta)}{\theta} \tag{61}$$

in the wet zone and

$$\theta = (\theta_L - \bar{\theta})\frac{\xi - \bar{\xi}}{1 - \bar{\xi}} + \bar{\theta}, \tag{62}$$

$$c^2 = \frac{1}{\theta^2}\left(\bar{\theta}^2\bar{c}^2 + \frac{\theta_L^2 c_L^2 - \bar{\theta}^2\bar{c}^2}{(\theta_L(\xi - \bar{\xi})^2 + \bar{\theta})(1 - \bar{\xi})}\left(\theta_L + \bar{\theta}(2 - \bar{\xi} - \xi)(\xi - \bar{\xi})\right)\right), \tag{63}$$

$$c_1 = c\left(\frac{v_G}{\delta_G}(c\theta - c_L\theta_L) - \log\left(\frac{c_{2L}}{c_L}\right) - \log\phi\right) \tag{64}$$

in the dry zone. The fluxes in (50) and (51) are defined by

$$F_G = v_G\epsilon(c + c_1)(c\theta)_\xi\,, \quad F_T = v_T\epsilon\theta(c\theta)_\xi + \delta_T\kappa_T\theta_\xi\, s.$$

Since the solutions and flux are continuous, it is easy to see that the solutions satisfy the following continuity conditions at the interface $\xi = \bar{\xi}$

$$[\theta] = 0, \quad [c_1] = 0, \quad [c] = 0, \quad [F_T] = 0, \quad [\theta_\xi] = 0.$$

Now we use these conditions to determine the matching point $(\bar{\xi}, \bar{\theta})$.

At the dry zone, by (46)

$$v_T\epsilon\theta(c\theta)_\xi + \delta_T\kappa_T\theta_\xi = F_T = \text{constant}. \tag{65}$$

Since θ is a linear function, multiplying $1/\theta$ in both sides of the above equation and integrating from $\bar{\xi}$ to 1, we have

$$v_T\epsilon\left(c_L\theta_L - \bar{c}\bar{\theta}\right) + \delta_T\kappa_T\log\left(\frac{\theta_L}{\bar{\theta}}\right) = \frac{F_T}{\theta_\xi(\bar{\xi})}\log\left(\frac{\theta_L}{\bar{\theta}}\right).$$

In the wet zone, by (47),

$$v_G(c\theta)_\xi = -\delta_G\left(\log\left(\frac{c\theta - c_1\theta}{\phi c\theta}\right)\right)_\xi = -\delta_G\left(\frac{(c\theta)_\xi - p_{s,\xi}\theta_\xi}{c\theta - p_s} - \frac{(c\theta)_\xi}{c\theta}\right),$$

which leads to

$$(c\theta)_\xi = \frac{\delta_G}{v_G}\frac{p_{s,\xi}(\theta)}{(c\theta - p_s(\theta))}\theta_\xi, \tag{66}$$

where we have used (60) and noting $\delta_G \ll v_G$. Thus

$$F_T = \left(\frac{\delta_G v_T\epsilon}{v_G}\frac{\bar{\theta}\,p_{s,\xi}(\bar{\theta})}{\bar{c}\bar{\theta} - p_s(\bar{\theta})} + \delta_T\kappa_T\right)\theta_\xi(\bar{\xi}).$$

It follows from continuity conditions that

$$\left(\frac{\delta_G v_T \epsilon}{v_G}\frac{\bar{\theta} p_{s,\xi}(\bar{\theta})}{\bar{c}\bar{\theta} - p_s(\bar{\theta})} + \delta_T \kappa_T\right) = \frac{v_T \epsilon \left(c_L \theta_L - \bar{c}\bar{\theta}\right) + \delta_T \kappa_T \log\left(\frac{\theta_L}{\bar{\theta}}\right)}{\ln\left(\frac{\theta_L}{\bar{\theta}}\right)},$$

which is simplified as

$$\frac{c_{1L}}{c_L} - \frac{p_s(\bar{\theta})}{c_L \theta_L} = \frac{\bar{\theta} p_{s,\xi}(\bar{\theta})}{(\bar{c}\bar{\theta} - p_s(\bar{\theta}))} \log\left(\frac{\theta_L}{\bar{\theta}}\right) \tag{67}$$

by using (60), where $\bar{c}$ is calculated by (60). Solving the above equation gives $\bar{\theta} = 1.026$.

To determine $\bar{\xi}$, we use the continuity condition $[\theta_\xi] = 0$. By (57)

$$\left(\frac{2\delta_G \epsilon}{\beta_G} p_{s,\xi}(\bar{\theta}) + \frac{2\delta_T \kappa_T}{\beta_T}\theta\right)\theta_\xi = \frac{2\delta_G \epsilon}{\beta_G}\frac{p_s(\bar{\theta}) - p_s(\theta_H)}{\bar{\theta}^2 - \theta_H^2}\frac{\bar{\theta}(\bar{\theta} - \theta_H)}{\bar{\xi}} + \frac{2\delta_T \kappa_T}{\beta_T}\frac{\bar{\theta}(\bar{\theta} - \theta_H)}{\bar{\xi}}$$

at $\theta = \bar{\theta}^-$. Since $\theta_\xi(\bar{\xi}^+) = (\theta_L - \bar{\theta})/(1 - \bar{\xi})$, we have

$$\left(\frac{2\delta_G \epsilon}{\beta_G} p_{s,\xi}(\bar{\theta}) + \frac{2\delta_T \kappa_T}{\beta_T}\theta\right)\frac{\theta_L - \bar{\theta}}{1 - \bar{\xi}} = \frac{2\delta_G \epsilon}{\beta_G}\frac{p_s(\bar{\theta}) - p_s(\theta_H)}{\bar{\theta}^2 - \theta_H^2}\frac{\bar{\theta}(\bar{\theta} - \theta_H)}{\bar{\xi}} + \frac{2\delta_T \kappa_T}{\beta_T}\frac{\bar{\theta}(\bar{\theta} - \theta_H)}{\bar{\xi}}. \tag{68}$$

Solving the above linear equation, we obtain $\bar{\xi} = 0.827$, based on the parameter values in Table 2.

Remark The quasi-steady-state solution obtained here provides some useful insight into the physical process involved in moisture transport in clothing assemblies. It can also be used as a benchmark or numerical solutions.

3.2 Numerical method

As discussed earlier, we will decouple the water absorption by fiber from the moisture transport and energy equation. In the governing equations, we will neglect water absorption by fiber as it happens at a much slower time scale. The water absorption by fiber will be computed separately.

Since the equations are of the convection–diffusion–reaction equations, normally, one uses explicit treatment for the convective term (involving velocity), implicit time-stepping for the diffusion term and the reaction term. However, it was shown that this will lead to an inefficient numerical scheme with a extremely small time-step [21]. The main reason is that the convection in the set of equations studied here behave as diffusion.

In order to see this, substitute Darcy's law in the equations for vapor and air and add the two, which leads to

$$\frac{\partial \epsilon c}{\partial \tau} - \frac{\partial}{\partial \xi}\left(v_G \epsilon c \frac{\partial c\theta}{\partial \xi}\right) = -\beta_G S, \tag{69}$$

where $c = c_1 + \phi c_2$ is the nondimensional total concentration. Therefore, we need to treat the convective term as a diffusive term in the equation of the mixture.[1] Numerically, it may be advantageous to use the nondimensional pressure $p = c\theta$ as a main variable instead of c and the governing equations are

$$\frac{\partial}{\partial \tau}\left(\frac{\epsilon}{\theta} p\right) = \frac{\partial}{\partial \xi}\left(v_G \epsilon \frac{p}{\theta}\frac{\partial p}{\partial \xi}\right) - \beta_G S, \tag{70}$$

$$\frac{\partial}{\partial \tau}(\epsilon c_1) - \frac{\partial}{\partial \xi}\left(v_G \epsilon c_1 \frac{\partial p}{\partial \xi}\right) = \frac{\partial}{\partial \xi}\left(\delta_G \epsilon \frac{p}{\theta}\frac{\partial}{\partial \xi}\left(\frac{\theta}{p} c_1\right)\right) - \beta_G S, \tag{71}$$

$$\frac{\partial}{\partial \tau}(c_{vl}\theta) = \frac{\partial}{\partial \xi}\left(v_T \epsilon \theta \frac{\partial p}{\partial \xi}\right) + \frac{\partial}{\partial \xi}\left(\delta_T \kappa_T \frac{\partial \theta}{\partial \xi}\right) + \beta_T S, \tag{72}$$

[1] We note that, if air motion is not taken into account, the equation of the mixture is the same as that of the vapor. Thus, the convective term in the vapor equation should be treated the same way as the diffusive term. However, this is not necessary here.

which are strongly coupled. The coupling of the liquid water equation is much weaker (through coefficients)

$$\frac{\partial}{\partial\tau}\left(\rho_{fw}(1-\epsilon')\widetilde{W}\right)-\frac{\partial}{\partial\xi}\left(v_W\widetilde{W}^3J_s(s)\frac{\partial\widetilde{W}}{\partial\xi}\right)=\frac{\partial}{\partial\xi}\left(\delta_W\rho_{fw}(1-\epsilon')\frac{\partial\widetilde{W}}{\partial\xi}\right)+\beta_W S. \tag{73}$$

The source term S in Eq. (70) will be treated implicitly in p by a rearrangement as follows

$$S=(1-\epsilon')\sqrt{1+\rho_{fw}\widetilde{W}}\frac{p}{\sqrt{\theta}}-(1-\epsilon')\sqrt{1+\rho_{fw}\widetilde{W}}\frac{\phi c_2\theta+p_s(\theta)}{\sqrt{\theta}}. \tag{74}$$

Using p as a main variable, we rewrite the boundary conditions at $\xi=0$ as

$$v_G\epsilon\frac{p}{\theta}\frac{\partial p}{\partial\xi}=\alpha_{c_{1H}}(c_1-c_{1H})+\alpha_{c_{2H}}\phi(c_2-c_{2H}), \tag{75}$$

$$v_G\epsilon c_1\frac{\partial p}{\partial\xi}+\delta_G\epsilon\frac{p}{\theta}\frac{\partial}{\partial\xi}\left(\frac{\theta c_1}{p}\right)=\alpha_{c_{1H}}(c_1-c_{1H}), \tag{76}$$

$$v_T\epsilon\theta\frac{\partial p}{\partial\xi}+\delta_T\kappa_T\frac{\partial\theta}{\partial\xi}=\alpha_{T_H}(\theta-\theta_H), \tag{77}$$

$$v_W\widetilde{W}^3J_s(s)\frac{\partial\widetilde{W}}{\partial\xi}-\delta_W\rho_{fw}(1-\epsilon')\frac{\partial\widetilde{W}}{\partial\xi}=0, \tag{78}$$

where

$$\alpha_{c_{1H}}=\frac{1}{R_{c_{1H}}+1/h_{c_{1H}}},\quad \alpha_{c_{2H}}=\frac{1}{R_{c_{2H}}+1/h_{c_{2H}}},\quad \alpha_{T_H}=\frac{1}{R_{T_H}+1/h_{T_H}}.$$

At $\xi=1$, similarly we have

$$v_G\epsilon\frac{p}{\theta}\frac{\partial p}{\partial\xi}=\alpha_{c_{1L}}(c_{1L}-c_1)+\alpha_{c_{2L}}\phi(c_{2L}-c_2), \tag{79}$$

$$v_G\epsilon c_1\frac{\partial p}{\partial\xi}+\delta_G\epsilon\frac{p}{\theta}\frac{\partial}{\partial\xi}\left(\frac{\theta c_1}{p}\right)=\alpha_{c_{1L}}(c_{1L}-c_1), \tag{80}$$

$$v_T\epsilon\theta\frac{\partial p}{\partial\xi}+\delta_T\kappa_T\frac{\partial\theta}{\partial\xi}=\alpha_{T_L}(\theta_L-\theta), \tag{81}$$

$$v_W\widetilde{W}^3J_s(s)\frac{\partial\widetilde{W}}{\partial\xi}-\delta_W\rho_{fw}(1-\epsilon')\frac{\partial\widetilde{W}}{\partial\xi}=0, \tag{82}$$

where

$$\alpha_{c_{1L}}=\frac{1}{R_{c_{1L}}+1/h_{c_{1L}}},\quad \alpha_{c_{2L}}=\frac{1}{R_{c_{2L}}+1/h_{c_{2L}}},\quad \alpha_{T_L}=\frac{1}{R_{T_L}+1/h_{T_L}}.$$

We use a finite-difference approximation for the spatial and time discretization of the coupled equations (70)–(73). For the vapor concentration and temperature, we use implicit treatment for the diffusion term and convective term. For the total pressure, we treat the convective term implicitly since it behaves as a diffusive term. The condensation term in the temperature equation is linearized and treated implicitly. After the boundary conditions are discretized accordingly, the system of discrete equations are then solved using tridiagonal solver at each time step.

Remark Since we have treated the convective and reaction terms implicitly, we are able to use large time steps for the computation. As a result, the numerical method is very efficient.

4 Results

In this section we present the results obtained using our model. We start by comparing the numerical results with the quasi-steady state approximate solution under a simplified setting.

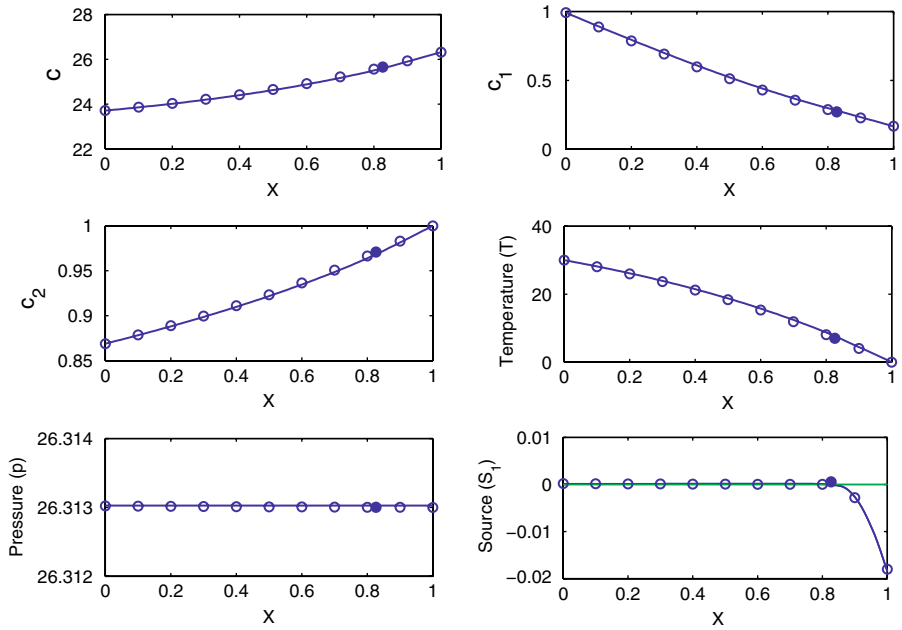

Fig. 2 The comparison between numerical and approximate solutions for 10 piles polyester batting sandwiched by two layers of laminated fabric where the solid line denotes the numerical solution with $\Delta\xi = 0.01$ ($\Delta x = 0.01L$) and • denotes the interface of dry and wet zones

4.1 Comparison between numerical and approximate solutions

The purpose of this section is to provide some evidences that our approximate solution given in Sect. 3.1 is consistent with the numerical solution when the quasi-steady state is reached. To simplify the discussion, we only restrict to the case where the outside temperature is set to be $T_L = 253\,\mathrm{K}$. In Fig. 2, we plot the numerical and quasi-steady approximate solutions for vapor concetration c_1, air concentration c_2, total concentrations c, temperature T, pressure p and the source distribution S_1, where

$$S_1 = c_1 - \frac{p_s(\theta)}{\theta^{3/2}}.$$

As shown by the figure, there is an interface between a dry zone (on the left) and a wet zone (on the right). The concentrations, temperature and pressure obtained by the two methods agree well. Therefore, the results confirm that the numerical method is reliable. Furthermore, our results also suggest that the solution reaches a quasi-steady state within a relatively short time (not shown here).

4.2 Condensation and water accumulation

As shown by the results in the previous section, the gas concentration, temperature and pressure reach the quasi-steady state within a short time period. The solution is quasi-steady since the water content is time-dependent due to condensation. We now present the comparison between the computed water content and the experimental measurements obtained in [22] for two different types of materials. The comparisons are given for 10 piles of polyester batting sandwiched by two thin layers of laminated fabric, at 8 and 24 h, as shown in Figs. 3 and 4. For illustrative purposes, we also plot the concentration, temperature, pressure, gas velocity and the source of condensation. It can be observed in Fig. 3 that the spatial water content variation resembles that of the source profile, which seems to indicate that the water accumulation can be approximated by taking the quasi-steady solution and integrated over the time period. However, a close inspection of the water content and source profile suggests that the spatial variation

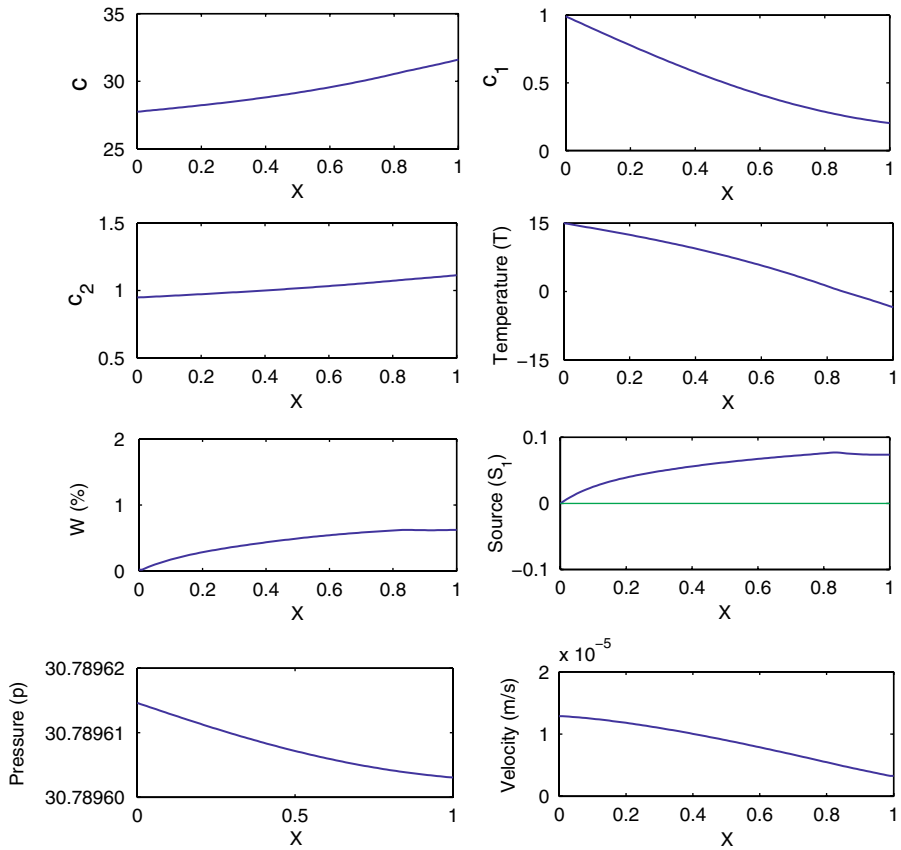

Fig. 3 Numerical results for 10 piles polyester batting sandwiched by two layers of laminated fabric at 8 hours

of the two quantities are not always correlated at the 24 h mark. The decrease in accumulated water content near the outer boundary is more significant than that of the source profile. It is interesting to note that the profound decrease in the accumulated water content predicted by our model agrees well with the experimental result in Fig. 5, which is not the case for numerical results obtained by single-component models [19,21].

In Figs. 6 and 7, a comparison is given for a clothing assembly with 10 piles of polyester batting sandwiched by two nylon fabric, at 8 and 24 h mark. Since nylon fabric is more permeable to air and vapor movement, it allows more influx of vapor from the artificial skin. On the other hand, nylon also allows more air and vapor to escape through the outer layer, which results in a larger mixture velocity. Thus, it is not clear whether less or more condensation may occur. Our numerical results show that the overall water accumulation is more for the nylon cover, suggesting that the dominant factor for water condensation is perhaps the influx of vapor. This result is consistent with the experimental observation, as shown by Fig. 8.

From a computational point of view, the difference between nylon and laminated covers is in the boundary condition. For laminated covers, the coefficients in the boundary conditions are given by $\alpha_{c_{1L}} = 0.0147$, $\alpha_{c_{2L}} = 0$, $\alpha_{T_L} = 4.42 \times 10^{-5}$, $\alpha_{c_{1H}} = 49.1$, $\alpha_{c_{2H}} = 0$, $\alpha_{T_H} = 1.77 \times 10^5$ while for nylon cover, we have $\alpha_{c_{1L}} = \phi\alpha_{c_{2L}} = 0.0196$, $\alpha_{T_L} = 6.01 \times 10^{-5}$, $\alpha_{c_{1H}} = \phi\alpha_{c_{2H}} = 49.1$, $\alpha_{T_H} = 1.77 \times 10^5$.

Finally, it is interesting to note that the amount of accumulated water, recorded by the experiments, shows a non-smooth behavior where the total water accumulation increases initially from the inner to the outer boundaries but decreases in the region close to the outer boundary. This behavior is also captured by our numerical solutions.

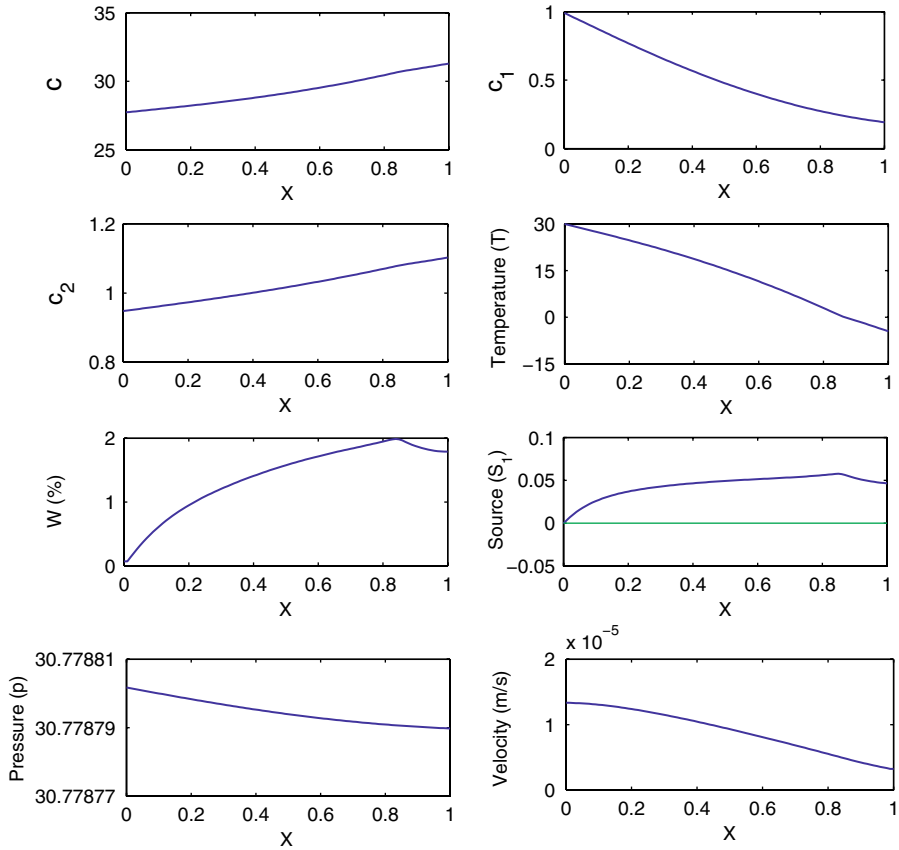

Fig. 4 Numerical results for 10 piles polyester batting sandwiched by two layers of laminated fabric at 24 h

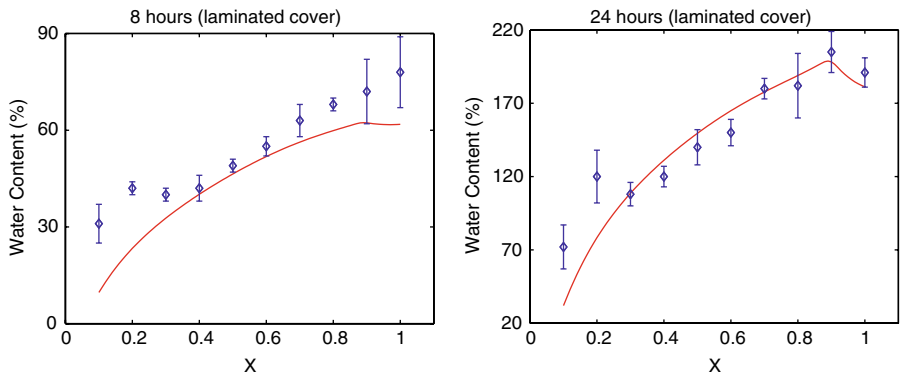

Fig. 5 The comparison of water contents with experimental measurements (two layers of laminated fabric)

4.3 Water absorption by fiber

In principle, the amount of water absorption by fiber can be computed by solving the diffusion equation discussed in Sect. 2. However, since the diffusion of water in fiber occurs at a much longer time scale, direct computation at each time step is time-consuming and unnecessary. We will use a simpler but much faster approach in this study based on the observation that water vapor reaches a pseudo-steady state quickly. Therefore, we will solve the diffusion equation for fiber absorption only once, using the pseudo-steady vapor solution as the boundary condition.

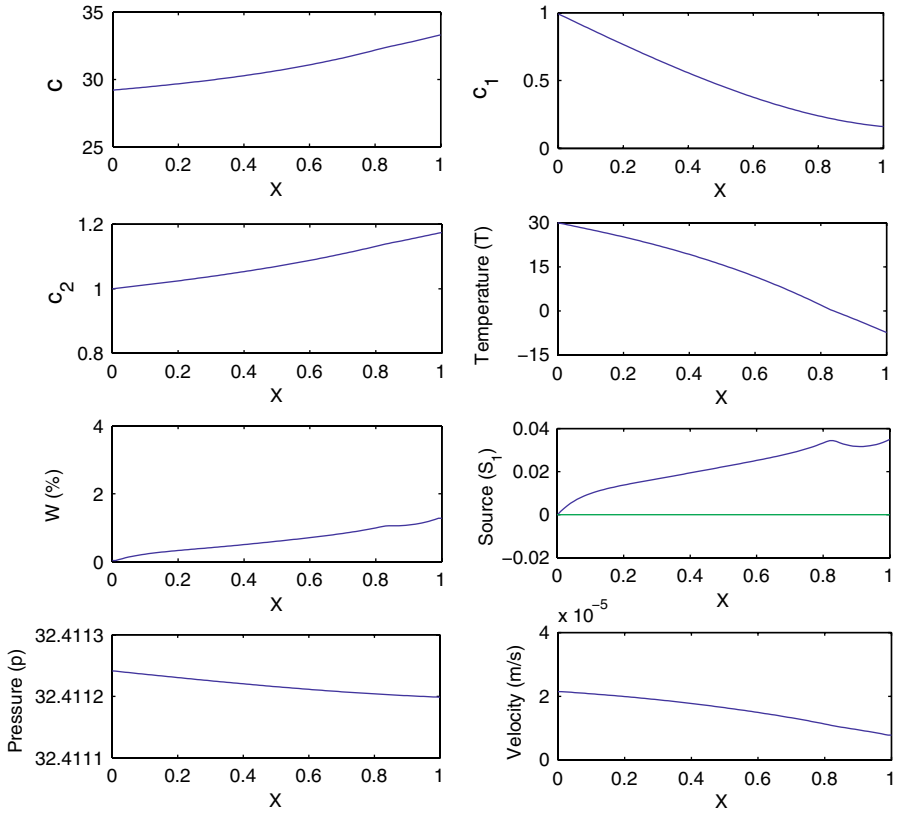

Fig. 6 Numerical results for 10 piles polyester batting sandwiched by two layers of nylon fabric at 8 h where $T(0.84) \approx 0$

If we neglect the effect of absorbed water on the thermal properties and the density of the porous assemblies, we can further simplify the problem by using the steady state solution, i.e., $c'_f = \rho W'_B(RH)/(MC^i_v)$, where $W'_B(RH)$ is based on the empirical data. The relative humidity RH is related to vapor content

$$RH = \frac{c_1\theta}{p_s}.$$

The water absorption by fiber can be calculated by

$$W_f = \frac{2MC^i_v}{\rho}\int_0^1 c'_f y\mathrm{d}y = 2W'_B(RH)\int_0^1 \bar{c}'_f y\mathrm{d}y = W'_B(RH)\bar{c}_f. \tag{83}$$

For polyester, $W'_B(RH) < 2\%$. The water absorption by fiber can be neglected and $W \approx \widetilde{W}$. For some other textile materials, such as wool fiber and viscose, $W'_B(RH) > 29\%$ [22] and the water absorption by fiber should be added in the total water content.

5 Conclusion

In this paper we have investigated a mathematical model for studying moisture transport in fibrous porous media. Our model is based on a previous multiphase model used in [19,21]. By examining the setup in [22] carefully, we postulate that the missing mechanism in the previous model [21,22] is the resistance provided by the air. The most significant modification made in this paper is to include a multi-component flavor by treating the air and vapor separately. Even though multi-component multiphase models were used elsewhere, they have not been used in the context of clothing assemblies as a fibrous porous medium or in a similar application area of insulating building

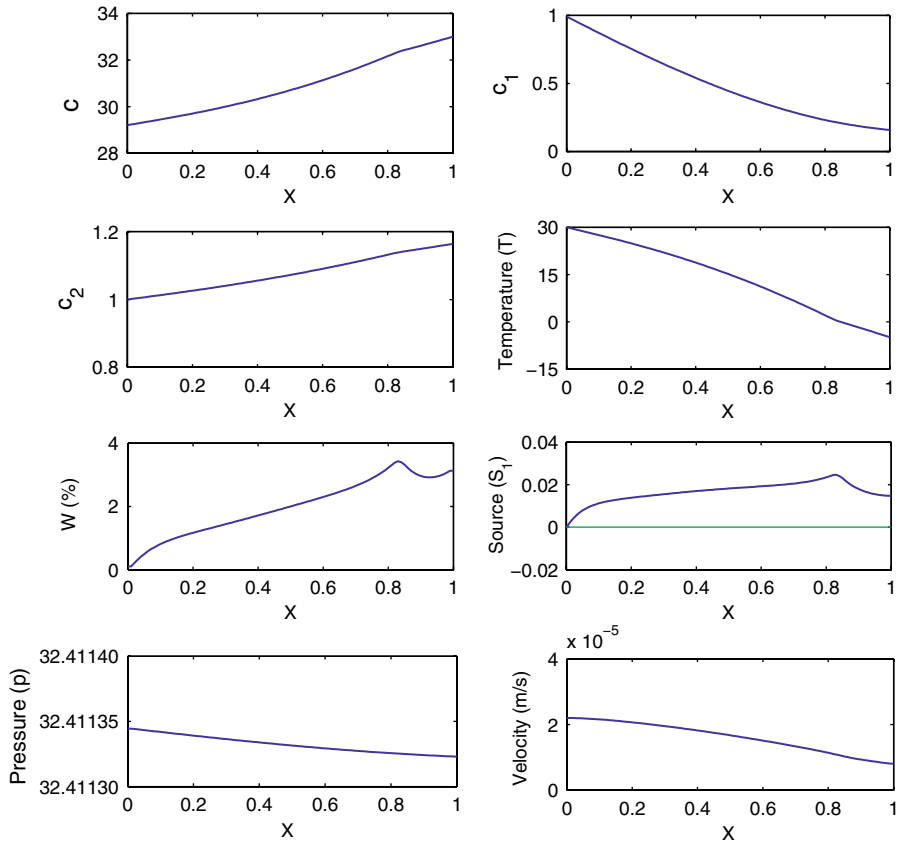

Fig. 7 Numerical results for 10 piles polyester batting sandwiched by two layers of nylon fabric at 24 h where $T(0.84) \approx 0$

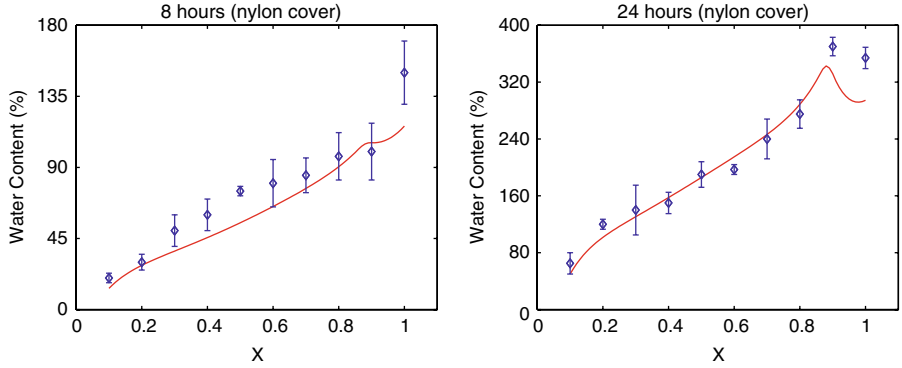

Fig. 8 The comparison of water contents with experimental measurements (two layers of nylon fabric)

materials. Qualitative comparison between the numerical results of our model and the experimental measurements done in [22] show that our model is more realistic.

Based on the physical and geometric setup of the problem, we show that there exist several separations of scales. In particular, the absorption of water by fiber occurs on a much slower time scale. Therefore, computing water content due to absorption can be decoupled from the rest of the calculation, which makes the computation much more efficient. Moreover, our approximate solution and numerical results also show that the physical process is quasi-steady, i.e., the gas concentration, temperature and pressure reach the steady state within a short time period

and the water content is time-dependent due to condensation. In addition, careful treatment of the convection term leads to an efficient numerical method, which allows us to compute the solution over a long time horizon much more quickly than the method used in previous studies [21].

Since the main focus of the paper is on the modeling of the process inside the batting layer, we have treated the cover layers using generic boundary conditions. This simplification is justified as the cover layers are much thinner than the batting layer. Nevertheless, it is desirable to extend the present study to three-layer clothing assemblies instead of the ad hoc approach used in this paper. This will allow us to study the effect of material properties of the batting layer as well as the cover layers on the transport of moisture.

Acknowledgements The authors would like to acknowledge the financial support from the Natural Science and Engineering Research Council (NSERC) of Canada, the MITACS NCE (Canada) and a grant from the Research Grants Council of the Hong Kong Special Administrative Region, China (Project No. CityU 101906). The authors wish to thank Professor J. Fan for helpful discussions.

References

1. Ghali K, Ghaddar N, Jones B (2002) Modeling of heat and moisture transport by periodic ventilation of thin cotton fibrous media. Int J Heat Mass Transfer 45:3707–3714
2. Foss WR, Bronkhorst CA, Bennett KA (2002) Simultaneous heat and mositure transport in paper sheets during moisture sorption from humid air. Int J Heat Mass Transfer 46:2875–2886
3. Wijeysundera NE, Zheng BF, Iqbal M, Hauptmann EG (1995) Numerical simulation of the transient moisture transfer through porous insulation. Int J Heat Mass Transfer 39:995–1004
4. Choudhary MK, Karki KC, Patankar SV (2004) Mathematical modeling of heat transfer, condensation, and capillary flow in porous insulation on a cold pipe. Int J Heat Mass Transfer 47:5629–5638
5. Stockie J, Promislow K, Wetton BR (2003) A finite volume method for multicomponent gas transport in a porous fuel cell electrode. Int J Numer Meth Fluids 41:577–599
6. Henry PSH (1948) Diffusion of moisture and heat through textiles. Discuss Faraday Soc 3:243–257
7. Farnworth B (1986) A numerical model of the combined diffusion of heat and water vapor through clothing. Tex Res J 56:653–665
8. Motakef S, El-Masri MA (1986) Simultaneous heat and mass transfer with phase change in a porous slab. J Heat Mass Transfer 29:1503–1512
9. Murata K (1995) Heat and mass transfer with condensation in a fibrous insulation slab bounded on one side by a cold surface. Int J Heat Mass Transfer 38:3253–3262
10. Ogniewicz Y, Tien CL (1981) Analysis of condensation in porous insulation. J Heat Mass Transfer 24:421–429
11. Shapiro AP, Motakef S (1990) Unsteady heat and mass transfer with phase change in porous slab: analytical solutions and experimental results. J Heat Mass Transfer 33:163–173
12. Smith P, Twizell ET (1984) A transient model of thermoregulation in a clothed human. Applied Math Model 8:211–216
13. Tao YX, Besant RW, Rezkallah KS (1991) Unsteady heat and mass transfer with phase changes in an insulation slab: frosting effects. Int J Heat Mass Transfer 34:1593–1630
14. Tao YX, Besant RW, Rezkallah KS (1992) The transient thermal response of a glass-fiber insulation slab with hygroscopic effects. Int J Heat Mass Transfer 35:1155–1167
15. Vafai K, Sarkar S (1986) Condensation effects in a fibrous insulation slab. J Heat Transfer 108:667–675
16. Vafai K, Tien HC (1989) A numerical investigation of phase change effects in porous materials. Int J Heat Mass Transfer 32:1261–1277
17. Promislow K, Stockie J (2001) Adiabatic relaxation of convective-diffusive gas transport in a porous fuell cell electrode. SIAM J Appl Math 62:180–205
18. Nam JH, Kaviany M (2003) Effective diffusivity and water-saturation distribution in single- and two-layer PEMFC diffusion medium. Int J Heat Mass Transfer 46:4595–4611
19. Fan J, Luo Z, Li Y (2000) Heat and moisture transfer with sorption and condensation in porous clothing assemblies and numerical simulation. Int J Heat Mass Transfer 43:2989–3000
20. Fan J, Wen X (2002) Modelling heat and moisture transfer. Int J Heat Mass Transfer 45:4045–4055
21. Fan J, Cheng X, Wen X, Sun W (2004) An improved model of heat and moisture transfer with phase change and mobile condensates in fibrous insulation and comparison with experimental results. Int J Heat Mass Transfer 47:2343–2352
22. Fan J, Cheng X, Chen Y-S (2003) An experimental investigation of moisture absoption and condensation in fibrous insulations under low temperature. Exp Thermal Fluid Sci 27:723–729
23. Taylor R, Krishna R (1993) Multicomponent mass transfer. John Wiley & Sons Inc, New York
24. Jones FE (1992) Evaporation of water. Lewis Publishers Inc., Michigan
25. Promislow K, Stockie J, Wetton BR (2006) A sharp interface reduction for multiphase transport in a porous fuel cell electrode. Proc R Soc Lond A 462((2067):789–816